Free Radical Biology and Medicine 94 (2016) 99–109

Contents lists available at ScienceDirect

Free Radical Biology and Medicine

journal homepage: www.elsevier.com/locate/freeradbiomed

Original Contribution

Interaction of singlet oxygen with bovine serum albumin and the role of the protein nano-compartmentalization

Rodrigo E. Giménez [a], Veronika Vargová [c], Valentina Rey [a], M. Beatriz Espeche Turbay [a], Inés Abatedaga [a], Faustino E. Morán Vieyra [a], Verónica I. Paz Zanini [a], Juan H. Mecchia Ortiz [b], Néstor E. Katz [b], Veronika Ostatná [c], Claudio D. Borsarelli [a,*]

[a] Instituto de Bionanotecnología, INBIONATEC-CONICET, Universidad Nacional de Santiago del Estero (UNSE), RN9, Km 1125, G4206XCP Santiago del Estero, Argentina
[b] INQUINOA-CONICET, Instituto de Química Física, Facultad de Bioquímica, Química y Farmacia, Universidad Nacional de Tucumán, Ayacucho 471, T4000INI San Miguel de Tucumán, Argentina
[c] Institute of Biophysics, Academy of Sciences of the Czech Republic, v.v.i., Královopolská 135, 612 65 Brno, Czech Republic

ARTICLE INFO

Article history:
Received 9 May 2015
Received in revised form
13 February 2016
Accepted 15 February 2016
Available online 17 February 2016

Keywords:
Tryptophan fluorescence
Singlet oxygen
Reactive oxygen species
Albumin
Protein oxidation
Photosensitization

ABSTRACT

Singlet molecular oxygen ($^1O_2$) contributes to protein damage triggering biophysical and biochemical changes that can be related with aging and oxidative stress. Serum albumins, such as bovine serum albumin (BSA), are abundant proteins in blood plasma with different biological functions. This paper presents a kinetic and spectroscopic study of the $^1O_2$-mediated oxidation of BSA using the tris(2,2′-bipyridine)ruthenium(II) cation $[Ru(bpy)_3]^{2+}$ as sensitizer. BSA quenches efficiently $^1O_2$ with a total (chemical + physical interaction) rate constant $k_t^{BSA} = 7.3(\pm 0.4) \times 10^8\ M^{-1}\ s^{-1}$, where the chemical pathway represented 37% of the interaction. This efficient quenching by BSA indicates the participation of several reactive residues. MALDI-TOF MS analysis of intact BSA confirmed that after oxidation by $^1O_2$, the mass protein increased the equivalent of 13 oxygen atoms. Time-resolved emission spectra analysis of BSA established that Trp residues were oxidized to *N′*-formylkynurenine, being the solvent-accessible W134 preferentially oxidized by $^1O_2$ as compared with the buried W213. MS confirmed oxidation of at least two Tyr residues to form dihydroxyphenylalanine, with a global reactivity towards $^1O_2$ six-times lower than for Trp residues. Despite the lack of MS evidences, kinetic and chemical analysis also suggested that residues other than Trp and Tyr, *e.g.* Met, must react with $^1O_2$. Modeling of the 3D-structure of BSA indicated that the oxidation pattern involves a random distribution of $^1O_2$ into BSA; allowing also the interaction of $^1O_2$ with buried residues by its diffusion from the bulk solvent through interconnected internal hydrophilic and hydrophobic grooves.

1. Introduction

The harmful effects of reactive oxygen species (ROS) in cellular targets such as DNA, lipids, and proteins, have been linked to aging and degenerative diseases [1,2]. Proteins are by far the main components in cells and tissues, and are also the most reactive biological components against ROS [3], turning them into major targets of oxidative stress processes. Among ROS, singlet oxygen $^1O_2$ is a non-radical, non-polar and neutral excited state species of ground state molecular oxygen $^3O_2$ produced in biological systems by chemical, enzymatic, and photosensitized reactions [4–6]. The interaction of $^1O_2$ with amino acid side-chains can occur by both physical quenching and chemical reaction [7,8]. The former process results in nonradioactive relaxation of $^1O_2$ without chemical change in the amino acid residue. In contrast, the chemical pathway implies the addition of electrophilic $^1O_2$ to electron-rich amino acid residues such as Trp, Tyr, Cys, Met, and His with reaction rate constants $\approx 10^6$-$10^7\ M^{-1}\ s^{-1}$ [8]. Consequently, the biophysical and biochemical properties of oxidized proteins by $^1O_2$ are significantly altered, causing several adverse effects such as increased susceptibility to proteolytic enzymes, conformational and structural changes (altered light scattering, optical rotation, and ligand binding properties, unfolding, aggregation, etc),

Abbreviations: AA, amino acid residue; ADPA, anthracene-9,10-dipropionic acid disodium salt; BSA, bovine serum albumin; $^1O_2$, singlet molecular oxygen; DAS, decay associated spectra; DOPA, dihydroxyphenylalanine; HSA, human serum albumin; MLCT, metal-to-ligand charge-transfer; ROS, reactive oxygen species; SA, serum albumins; $[Ru(bpy)_3]^{2+}$, tris(2,2′-bipyridine), ruthenium(II) cation

* Corresponding author.
E-mail address: cdborsarelli@gmail.com (C.D. Borsarelli).

http://dx.doi.org/10.1016/j.freeradbiomed.2016.02.014
0891-5849/

crosslinking, and loss of enzymatic activity [9,10].

Serum albumins (SA) are the most abundant circulating proteins in blood plasma ($\approx 600\ \mu M$) playing several roles such as in intravascular and interstitial colloid pressure, modulation of capillary permeability, neutrophil adhesion, binding and transport of both endogenous and exogenous molecules, such as fatty acids, cholesterol, bile pigments, hormones, amino acids, peptides, therapeutic drugs and metal ions [11,12]. The secondary structure of SA is mainly α-helical (72–75%), comprising three homologous domains I–III, which are divided in two distinct subdomains (A and B) possessing common structural motifs [12,13].

Recent studies *in vivo* demonstrated the capability of the single free C34 residue of subdomain IA of human serum albumin (HSA) for free radical scavenging in extracellular body fluids, e.g. plasma, cerebrospinal and synovial fluids [14–17]. HSA also binds cytotoxic degradation metabolites, like homocysteine, oxysterols, iron (thereby preventing the Fenton reaction with endogenous hydrogen peroxide), and antioxidant biomolecules like bilirubin, inhibiting lipid peroxidation [15,16,18]. Moreover, oxidized HSA is considered as an oxidative stress biomarker for early diagnosis and monitoring of chronic and degenerative diseases [18]. Altogether, these functions make HSA (and SA in general) a multifunctional protein with also a role in oxidative stress processes.

In the photosensitized oxidation of SA, it has been shown that the sensitizer molecule localization in the protein plays a role in its photophysical and photochemical properties, as well as in the distribution of oxidation products, depending on the prevalence of charge-transfer oxidation processes (Type I) or $^1O_2$-mediated oxidation (Type II) [19–23].

In this work we report a kinetic and spectroscopic study of the oxidation of BSA by specifically $^1O_2$ in neutral buffer solutions using tris(2,2′-bipyridine)ruthenium(II) cation $[Ru(bpy)_3]^{2+}$ as photosensitizer. Kinetic, spectroscopic, chemical, and modeling data were analyzed to explain both the BSA reactivity towards $^1O_2$ and the effect of the protein nano-heterogeneity on the oxidation pattern of the protein.

2. Experimental

2.1. Materials

All chemicals were analytical purity grade products of Sigma-Aldrich Argentina (Buenos Aires, Argentina), and were used as received. All solutions were prepared in 50 mM sodium phosphate pH 7.4 buffer solution using triply distilled water at 25 °C, except for experiments of near-infrared luminescence detection of singlet molecular oxygen, $^1O_2$, for which D_2O (pD 7.4 adjusted with DCl using a recalibrated glass electrode [24]) was used as solvent to improve the $^1O_2$ signal detection. Compressed ultrapure argon (99.99%) was purchased from Indura SRL (S.M. de Tucumán, Argentina).

2.2. Steady-state photolysis experiments

A home-made steady-state photolysis system was built by focusing a blue LED (443 ± 21 nm, 1 W) as selective excitation source of $[Ru(bpy)_3]^{2+}$. Simultaneously, the absorption spectral changes of the solution were registered with the CCD-USB2000 UV–vis spectrometer (OceanOptics, Dunedin, FL, USA), with the analyzing UV–vis beam placed at right angle of the photolysis beam from the blue LED. Soft mixing of the solution was done with a magnetic stirring bar to avoid foam formation in the protein solutions.

Oxygen uptake kinetics were done with the same photolysis set-up, but by placing into a sealed 1 cm quartz cuvette (Hellma, Müllheim, Germany) either a micro-dissolved-O_2 electrode (DO-166MT-1, LAZAR Research Laboratories, Los Angeles, CA), or a FOXY-R-AF luminescent sensor tip coupled by fiber optic with a CCD-USB2000 fluorometer (OceanOptics).

2.3. Steady-state spectroscopies

UV–vis absorption spectra were registered using either a Hewlett Packard 8453 (Palo Alto, CA, USA) or the OceanOptics USB2000 UV–vis spectrophotometer. Luminescence emission measurements, in emission or excitation mode, were done with a Hitachi F-2500 (Kyoto, Japan) spectrofluorometer, equipped with a red-extended R-928 photomultiplier. All spectroscopic experiments were performed by triplicate at $25(\pm 1)$ °C in optical fused silica cuvettes of either 3 mm or 10 mm optical path (Hellma).

2.4. Time-resolved spectroscopies

Luminescence decays of $[Ru(bpy)_3]^{2+}$ were collected with the Tempro-01 spectrofluorometer of Horiba (Glasgow, UK) operating in the time-correlated single photon counting (TCSPC) mode. As excitation source a 250 kHz Nanoled® emitting at $461(\pm 27)$ nm was used. Photon detection was done with a −30 °C cooled TBX-07C PMT detector with < 10 dark counts placed in the output of an f/4 emission monochromator calibrated at the emission maximum. A diluted Ludox® scatter solution was used to register the instrumental response at the excitation wavelength and also to verify that no excitation scattered light was acquired at the emission wavelength. The luminescence intensity decays were fitted with the Fluorescence Decay Analysis Software DAS6® from Horiba by deconvolution of the pulse function using the multi-exponential model function as follows:

$$I(t) = \sum_{i=1}^{n} \alpha_i \exp(-t/\tau_i) \quad (1)$$

where n is the number of single exponential decays, τ_i and α_i are the decay time and the fluorescence intensity amplitude at $t=0$ of each decay, respectively. Time-resolved emission spectra (TRES) of native and oxidized BSA samples were also obtained with the Tempro-01 apparatus with Nanoled® excitation at $295(\pm 14)$ nm operating at 1 MHz. The sets of fluorescence decays as a function of the emission wavelength, with steps of 5 nm, were adjusted using the global fitting analysis option provided by the DAS6® software, to obtain the wavelength-dependent pre-exponential factor $\alpha_i(\lambda)$ associated with τ_i decay time. Thus, the Decay Associated Spectra (DAS) were calculated with

$$I_i(\lambda) = f_i(\lambda) I_{ss}(\lambda) = \frac{\alpha_i(\lambda)\tau_i}{\sum_i \alpha_i(\lambda)\tau_i} I_{ss}(\lambda) \quad (2)$$

where $I_{ss}(\lambda)$ is the steady-state emission spectrum and $f_i(\lambda)$ is the fractional contribution of each decay time for a particular emission wavelength.

Transient luminescence detection of $^1O_2$ experiments in air-saturated D_2O solutions were performed using a Minilite II Nd-YAG laser (Continuum Inc., San Clara, CA, USA) generating 355 nm pulses (fwhm 7 ns) as excitation source of the sensitizer $[Ru(bpy)_3]^{2+}$. A Ge photodiode J16TE2-66G from Teledyne Judson Technology (Montgomeryville, PA, USA) in combination with a band path filter (Spectrogon BP-1260, Sweden) was used to collect the weak luminescence of $^1O_2$ with a Tektronix TDS3032B oscilloscope (Beaverton, OR, USA). The prompt spike in the luminescent signal produced by spurious luminescence of the complex or scattered laser light was subtracted with the residual signal obtained with a solution of $[Ru(bpy)_3]^{2+}$ containing NaN_3 in a concentration to totally quench the luminescence of $^1O_2$ [23]. Up to 50 single transient signals were collected and averaged to improve

signal-to-noise ratio before analysis. Since the rise time of $^1O_2$ was $\tau_{\Delta,r} < 400$ ns and almost two-order of magnitude shorter than its decay time $\tau_{\Delta,d}$, the latter was obtained from single-exponential fitting of the signal decay portion [4].

2.5. Protein analysis

The protein carbonyls and hydroperoxides quantification were performed as previously described [20], with colorimetric methods by reaction with 2,4-dinitrophenylhydrazine (DNPH) [25] and by ferrous oxidation-xylenol orange (FOX) [26], respectively. The production of free H_2O_2 was evaluated in photo-oxidized samples of BSA by oxidative coupling with 4-aminophenazone and phenol in the presence of peroxidase to yield a quinoneimine dye, a chromogen with maximum absorption at 505 nm [27]. The reactants were obtained from the reaction kit Colestat (Weiner Lab, Rosario, Argentina), and standard H_2O_2 solutions were used for calibration.

Polyacrylamide gel electrophoresis in the presence of sodium dodecyl sulfate (SDS-PAGE) in 12% gels for BSA samples before and after photo-oxidation by blue-LED excitation of $[Ru(bpy)_3]^{2+}$was performed using a Mini-Protean Tetra cell apparatus (Biorad, CA, USA), under reducing conditions and visualized with Coomassie blue.

2.6. MALDI-TOF mass spectrometry

Matrix assisted laser desorption ionization time-of-flight mass spectrometry (MALDI-TOF) experiments at the CEITEC—Central European Institute of Technology, Brno, Czech Republic, were recorded on an Ultraflextreme instrument (Bruker, Germany) operated in the linear mode with detection of positive ions. Ferulic acid (12.5 mg/ml in water:acetonitrile:formic acid, 50:33:17 v/v mixture) was used as the MALDI matrix. The spectra of intact 14.2 μM BSA, and of those containing 28.4 μM $[Ru(bpy)_3]^{2+}$ before and after 60 min of blue-light irradiation were obtained. These protein samples were also digested with trypsin and analyzed by MALDI-TOF-MS.

Further MS analysis of excised bands from native gels of 100 μM BSA with 20 μM $[Ru(bpy)_3]^{2+}$ before and after 60 min of blue-light irradiation were performed at the Proteomics Core Facility CEQUIBIEM, at the University of Buenos Aires (UBA) in Argentina. α-Cyano-4-hydroxycinnamic acid (3 mg/ml in 50% acetonitrile–0.5% trifluoroacetic acid v/v) was used as the MALDI matrix. MS data was collected in an Ultraflex II Buker Daltonic MALDI TOF/TOF equipment. The data was acquired in Reflectron positive mode using a detection mass range of 700–4000 Da, and 1250 laser shots were averaged for each mass spectrum. The equipment was calibrated with Bruker calibrant mixture Pep Mix II. The peak list was generated based on signal-to-noise filtering and an exclusion list of contaminants. Peaks observed in the different MS lists, were compared to the masses of the theoretical peptides originated in silico digestion of the protein sequence.

3. Results and discussion

3.1. Interaction of $[Ru(bpy)_3]^{2+}$ with $^3O_2$ and BSA

The interaction between the triplet excited metal-to-ligand charge-transfer state of tris(2,2′-bipyridine) ruthenium(II) cation $^*[Ru(bpy)_3]^{2+}$ and ground-state molecular oxygen $^3O_2$ has been extensively studied in several solvents [28–30]. Here, the quenching process in sodium phosphate at pH 7.4 at room temperature was revisited by steady-state and time-resolved fluorescence spectroscopy (data not shown), and a bimolecular

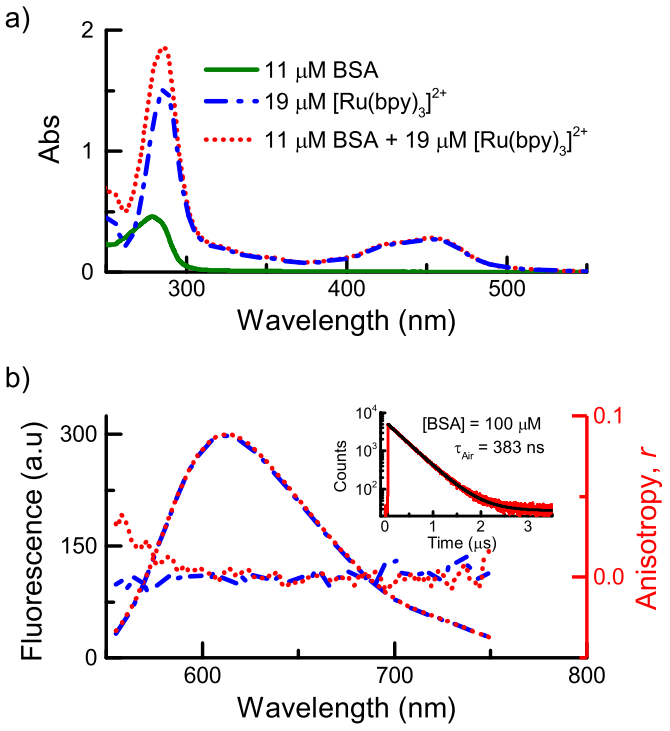

Fig. 1. (a) UV–vis absorption spectra of 11 μM BSA and 19 μM $[Ru(bpy)_3]^{2+}$ single and mixed solutions in 50 mM Na-phosphate buffer at pH 7.4. (b) Luminescence emission and anisotropy spectra of 7 μM $[Ru(bpy)_3]^{2+}$ in air-saturated 50 mM Na-phosphate buffer at pH 7.4 in absence (dashed lines) and presence of 100 μM BSA (dotted lines) obtained by excitation at 450 nm. Inset: luminescence decay of $[Ru(bpy)_3]^{2+}$ collected at 610 nm with Nanoled® excitation at 460 nm in presence of 100 μM BSA.

quenching rate constant $k_q = 3.5 \times 10^9\ M^{-1}\ s^{-1}$ was obtained, a similar value to that observed in neat water [30], indicating that the phosphate buffer does not alter the quenching process by neither environmental nor specific interaction effects.

Previous studies have demonstrated that the binding of sensitizer molecules to SA can strongly affect the photophysical pathways of the sensitizer by self-interaction and/or environmental effects as a consequence of compartmentalization of the sensitizer into the protein [21,23]. Therefore, the potential interaction between $[Ru(bpy)_3]^{2+}$ and BSA was evaluated. Fig. 1a shows that the UV–vis absorption spectrum of a solution containing both $[Ru(bpy)_3]^{2+}$ and BSA was almost identical to the sum of the individual spectra of each chromophore at the same concentration. The lack of new absorbance band(s) suggests the absence of ground state complex or adduct formed between $[Ru(bpy)_3]^{2+}$ and BSA. Additionally, the presence of 100 μM BSA in air-saturated solutions of $[Ru(bpy)_3]^{2+}$ did not alter neither the steady-state luminescence spectrum nor decay time of the $[Ru(bpy)_3]^{2+}$ complex (Fig. 1b), confirming that the albumin does not interact with the excited state of the complex and hence it does not alter the collisional quenching of $^*[Ru(bpy)_3]^{2+}$ by $^3O_2$. To confirm the lack of interaction between the complex and the albumin, the steady-state emission anisotropy of $[Ru(bpy)_3]^{2+}$ was evaluated in the presence of 100 μM BSA. The presence of protein did not change the anisotropy of the complex, which was $r \approx 0$ as expected for a molecular emitter with emission lifetimes τ much longer than its rotational correlation time θ in fluid solution [31]. Assuming a quantitative binding of the complex to BSA, *i.e.* binding constant value $K_b > 10^4\ M^{-1}$, it can be expected that the depolarization process of the bound complex is dominated by the rotation of the whole protein, with $\theta \approx 44 \pm 5$ ns for BSA [23]. In such hypothetical case, anisotropy increments of about 10% should be expected

according to the classical Perrin equation $r_0/r = 1+\tau/\theta$. Nevertheless, this was not the case, and a tight binding of $[Ru(bpy)_3]^{2+}$ to BSA can be ruled out, despite the fact that BSA bears an excess of negative charges at neutral pH [13].

Altogether, the above results confirm that neither ground nor excited state of the complex interacts with BSA under the present experimental conditions. This result agrees with the fact that only second-sphere modified Ru(II) bipyridine complexes containing hydrogen-bonding groups showed effective binding with BSA, but not for the parent Ru(II) complex [32].

3.2. Scavenging of $^1O_2$ by BSA: Chemical reaction and physical quenching pathways

The quenching of $^*[Ru(bpy)_3]^{2+}$ by $^3O_2$ in aqueous solutions produces $^1O_2$ with quantum yield Φ_Δ values between 0.22 and 0.50, depending on the dissolved oxygen concentration [28,30]. To confirm the Φ_Δ value under our experimental conditions, the laser-induced optoacoustic spectroscopy (LIOAS) technique was used [32], and $\Phi_\Delta = 0.29(\pm 0.03)$ was obtained in air-saturated sodium phosphate buffer [33], in agreement with $\Phi_\Delta = 0.22$ obtained in neat air-saturated water [28].

Fig. 2a shows the effect of BSA concentration on the $^3O_2$-uptake kinetics observed during steady-state photolysis with blue-LED light of air-saturated solutions of 20 μM $[Ru(bpy)_3]^{2+}$ placed in a sealed quartz cell with a microelectrode for dissolved oxygen (see Section 2). Control experiments of solutions containing 20 μM $[Ru(bpy)_3]^{2+}$ and 50 μM BSA (data not shown) demonstrated that $^3O_2$-uptake was not produced neither under dark conditions nor with large excess of sodium azide, a well-known physical quencher of $^1O_2$ [7], indicating that the depletion of dissolved oxygen was only produced by reaction of $^1O_2$ with BSA. Under constant photosensitization conditions of $[Ru(bpy)_3]^{2+}$ (photon flux, absorbance, temperature and irradiation geometry) and low conversion regime (< 10%) it can be assumed that the steady-state concentration of $^1O_2$ is constant. Thus, the initial rate of $^3O_2$-uptake $\nu_0^{O_2}$ is only dependent on the initial concentration of BSA, $[BSA]_0$, by reaction of $^1O_2$ with the protein. In fact, the double log plot of $\nu_0^{O_2}$ *vs.* $[BSA]_0$ was linear with slope ≈ 1 (Fig. 2b), confirming the above-mentioned assumption and a first-order dependence for the protein. Accordingly with the results of the previous section, the $[Ru(bpy)_3]^{2+}$ complex does not interact with BSA and $^1O_2$ is generated in the bulk solvent upon blue-LED irradiation of $[Ru(bpy)_3]^{2+}$ (Eqs. (3) and (4)). After its formation, $^1O_2$ decays unimolecularly to triplet ground state oxygen $^3O_2$ releasing heat and emitting weak near-infrared phosphorescence at 1270 nm [4] (Eq. (5)), competing with the bimolecular processes by interaction with BSA, i.e. chemical reaction pathway yielding oxidized protein BSA_{ox} (Eq. (6)), and physical quenching pathway deactivating $^1O_2$ to $^3O_2$ without modification of the protein (Eq. (7)).

$$[Ru(bpy)_3]^{2+} \xrightarrow{h\nu_{ex}} {}^*[Ru(bpy)_3]^{2+} \quad (3)$$

$${}^*[Ru(bpy)_3]^{2+} + {}^3O_2 \xrightarrow{k_q} [Ru(bpy)_3]^{2+} + {}^1O_2 \quad (4)$$

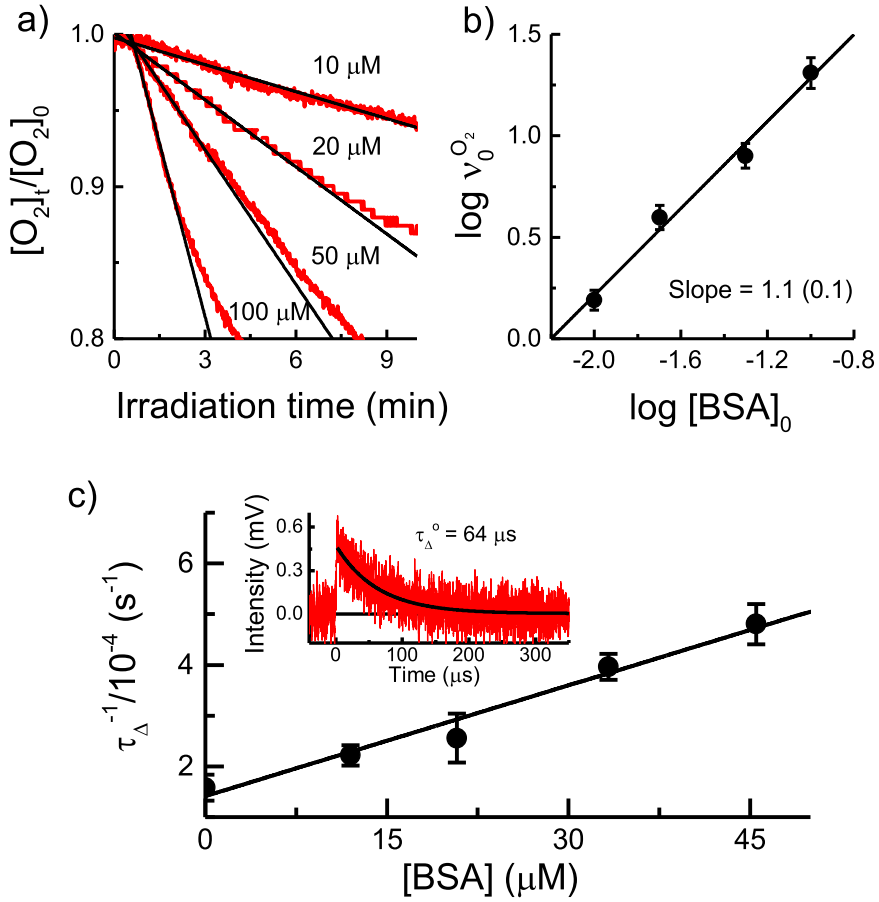

Fig. 2. (a) O_2-uptake kinetic as function of BSA concentration under steady-state irradiation with blue-LED (462 nm) of 20 μM $[Ru(bpy)_3]^{2+}$ in 50 mM Na-phosphate buffer at pH 7.4. (b) Double log plot of the initial rate of O_2-uptake $\nu_0^{O_2}$ *vs.* initial BSA concentration $[BSA]_0$. (c) Stern–Volmer plot for the total quenching of $^1O_2$ by BSA in neutral D_2O. Inset: luminescence decay of $^1O_2$ monitored at 1270 nm obtained after photosensitization of 40 μM $[Ru(bpy)_3]^{2+}$ with laser excitation at 352 nm (3 mJ/pulse) in air-saturated D_2O.

$$^1O_2 \xrightarrow{k_d = 1/\tau_\Delta^0} {}^3O_2 + \text{heat} + h\nu\,(1270\ \text{nm}) \quad (5)$$

$$^1O_2 + \text{BSA} \xrightarrow{k_c^{BSA}} (\text{BSA})_{ox} \quad (6)$$

$$^1O_2 + \text{BSA} \xrightarrow{k_p^{BSA}} {}^3O_2 + \text{BSA} \quad (7)$$

As both parallel bimolecular deactivation channels of $^1O_2$ are plausible in presence of BSA, *i.e.* (Eqs. (6) and (7)), the total quenching rate constant by BSA is given by $k_t^{BSA} = k_p^{BSA} + k_c^{BSA}$. The $^3O_2$-uptake kinetics by BSA were compared with those observed for a well-known $^1O_2$-trap as the water soluble anthracene-9,10-dipropionic acid disodium salt (ADPA), which exclusively reacts with $^1O_2$ to produce a stable endoperoxide at room temperature [34]. The bimolecular rate constant for the reaction of $^1O_2$ with ADPA of $k_c^{ADPA} = 7.4(\pm 0.5) \times 10^7\ M^{-1}\ s^{-1}$ was determined by time-resolved luminescence quenching experiments of $^1O_2$ in D_2O, the suitable solvent to improve the transient detection of $^1O_2$ with our experimental set-up (Fig. S1 of Supplementary Information).

$$^1O_2 + \text{ADPA} \xrightarrow{k_c^{ADPA}} \text{ADPAO}_2 \quad (8)$$

By considering the initial $^3O_2$-uptake rates under identical photosensitization conditions, the $k_c^{BSA} = 2.7(\pm 0.9) \times 10^8\ M^{-1}\ s^{-1}$ was calculated as follows [35]:

$$k_c^{BSA} = \frac{v_0^{BSA}}{v_0^{ADPA}} \times \frac{[\text{ADPA}]_0}{[\text{BSA}]_0} \times k_c^{ADPA} \quad (9)$$

The total quenching rate constant by BSA was calculated with Eq. (10), which accounts the shortening of the observed lifetime of $^1O_2$ (τ_Δ) due to the competition of both physical and chemical quenching by BSA with the unimolecular decay of $^1O_2$, (Eqs. (5)–(7)).

$$(\tau_\Delta)^{-1} = (\tau_\Delta^0)^{-1} + k_t^{BSA}[\text{BSA}] \quad (10)$$

The inset of Fig. 2c shows the transient luminescence signal of $^1O_2$ obtained by photosensitization of $[Ru(bpy)_3]^{2+}$ with laser excitation at 355 nm in D_2O solutions. In the absence of protein, a lifetime of $\tau_\Delta^\circ = 64 \pm 2$ μs was obtained by first-order fitting of the decay tail of $^1O_2$, as expected in D_2O solvent [4]. By increasing the concentration of BSA a shortening of τ_Δ was produced, and a $k_t^{BSA} = 7.3(\pm 0.4) \times 10^8\ M^{-1}\ s^{-1}$ was obtained by linear regression with Eq. (10). This k_t value was almost the same than that reported for the quenching of $^1O_2$ by HSA using the water soluble sensitizer phenalen-1-one-2-sulfonic acid (PNS) [36], confirming that human and bovine serum albumins show similar quenching efficiency of $^1O_2$, probably due to the large amino acid homology between them [13].

Both calculated k_c^{BSA} and k_t^{BSA} values are one-order of magnitude larger than those observed for the interaction of $^1O_2$ with free amino acids in buffer solutions at similar pH conditions [7,37–39]. This result indicates that several amino acid residues per BSA molecule contribute in parallel to both chemical and physical deactivation of $^1O_2$, *i.e.* $k_c^{BSA} = \sum_i k_{c,i}^{AA}$ and $k_t^{BSA} = \sum_i k_{t,i}^{AA}$. The comparison between k_c^{BSA} and k_t^{BSA} indicates that the interaction of $^1O_2$ with BSA is comprised of ≈40% of chemical reaction and ≈60% of physical quenching. The quenching of the electrophilic $^1O_2$ by electron-rich amino acids (AA), such as Trp, Tyr, His, Met and Cys, can be interpreted by formation of a singlet exciplex $^1(O_2^{\delta-} \cdots AA^{\delta+})$ [4,7,37], which can decay by intersystem crossing to a triplet charge-transfer (CT) complex $^3(O_2 \cdots AA)$ dissociating to the $^3O_2$ and AA, without chemical degradation of the amino acid, resulting in the physical quenching pathway (Eq. (7)). Nevertheless, the $^1(O_2^{\delta-} \cdots AA^{\delta+})$ exciplex can also form the oxidation product AAO_2 consuming dissolved $^1O_2$ (Eq. (6)). The latter reaction in proteins can produce side-chain carbonyls, hydroperoxides, sulfones and sulfoxides depending on the reactive AA [10,40].

The amino acid sequence of BSA contains besides the single free C34 (the rest of Cys residues are forming 17 disulfide bridges to keep tertiary structure) 2 Trp, 4 Met, 17 His, and 20 Tyr residues [13], which hypothetically can react with $^1O_2$ [10,40]. MALDI-TOF tests of tryptic digests obtained after native PAGE of 100 μM BSA and 20 μM $[Ru(bpy)_3]^{2+}$ before and after 60 min of blue-LED photolysis showed a set of very low intensity peaks with *m/z* suggesting peptides containing typical oxidations such as W (+4, +16, +20 and +32); Y and H (+16); M (+16 and +32); and C (+48) [41]. Nevertheless, due to sample treatment and the very low signals it was impossible to confirm their sequence by MS/MS experiments under the present experimental conditions.

However, independent MALDI-TOF experiments with larger sensitizer/protein ratio to reach more aggressive photo-oxidation conditions, e.g. 28.4 μM $[Ru(bpy)_3]^{2+}$ and 14.2 μM BSA, showed clear evidence of protein oxidation. Fig. 3a depicts that the mass spectrum of the intact BSA without and with the addition of $[Ru(bpy)_3]^{2+}$ and handled under dark condition were practically identical, with average mass MW = 66,433 Da, indicating that the metal complex does not modify the protein by undesirable thermal reactions. In contrast, after 60 min of blue-light irradiation of the solution containing both the protein and the complex, a mass increment of about 208 Da was observed, suggesting that at least 13 oxygen atoms were incorporated into the oxidized BSA, in perfect agreement with the kinetic data discussed above, *i.e.* $k_c^{BSA} \approx 10 k_{c,i}^{AA}$. After tryptic digestion, unequivocal evidence of oxygen atom addition (+16) was found in two peptides containing Y residues to form 3,4-dihydroxyphenylalanine (DOPA) with relative low intensity: (i) L^{397}GEYGFQNALIVR^{409} (*m/z* 1495.788) and (ii) D^{323}AFLGSFLYEYSR^{335} (*m/z* 1583.730) (Fig. S2 of Supplementary Information). Two more peptides were also detected, (iii) A^{212}WSVAR^{217} (*m/z* 721.30) that would correspond to the oxidation of W213 to *N′*-formylkynurenine (+32), and (iv) R^{336}HPEYAVSVLLR^{347} corresponding in this case, to the oxidation of H337 and Y340 most likely. However, the signal for the latter peptide was within the instrumental detection limit and therefore should be considered with caution.

Chemical analysis of the oxidized protein indicated that carbonyl residues ($R_2C{=}O$) on BSA were steadily formed during photosensitization with $[Ru(bpy)_3]^{2+}$, but not detectable amounts of side-chain hydroperoxides and/or free H_2O_2 were observed (Fig. 3b). The non-formation of free H_2O_2 is indicative of lack of charge-transfer processes (Type I mechanism) between BSA and the sensitizer $[Ru(bpy)_3]^{2+}$, as could be expected for tightly bound sensitizer to the albumin [20,42,43].

The observed initial rate of formation of carbonyls $v_0^{C=O}$ correlated linearly with that for $^3O_2$-uptake, *i.e.* $v_0^{O_2}$ (Fig. 3c), with a slope value suggesting that the formation of protein carbonyls represents ≈30% of the total $^1O_2$-mediated oxidation of BSA. Finally, the electrophoretic analysis by SDS-PAGE under denaturing conditions did not show any evidence of large structural protein alterations like fragmentation and/or cross-linking after photo-oxidation treatment (Fig. 3d), confirming the absence of charge-transfer processes between $^*[Ru(bpy)_3]^{2+}$ and some amino acid residues. Lack of structural changes after $^1O_2$-mediated oxidation of BSA using also $[Ru(bpy)_3]^{2+}$ as sensitizer was recently confirmed by label-free electrochemical measurements [44].

3.3. Role of Trp and Tyr residues on $^1O_2$ scavenging

During the blue-LED irradiation of $[Ru(bpy)_3]^{2+}$ in presence of BSA in air-saturated solutions, a continuous absorbance increment

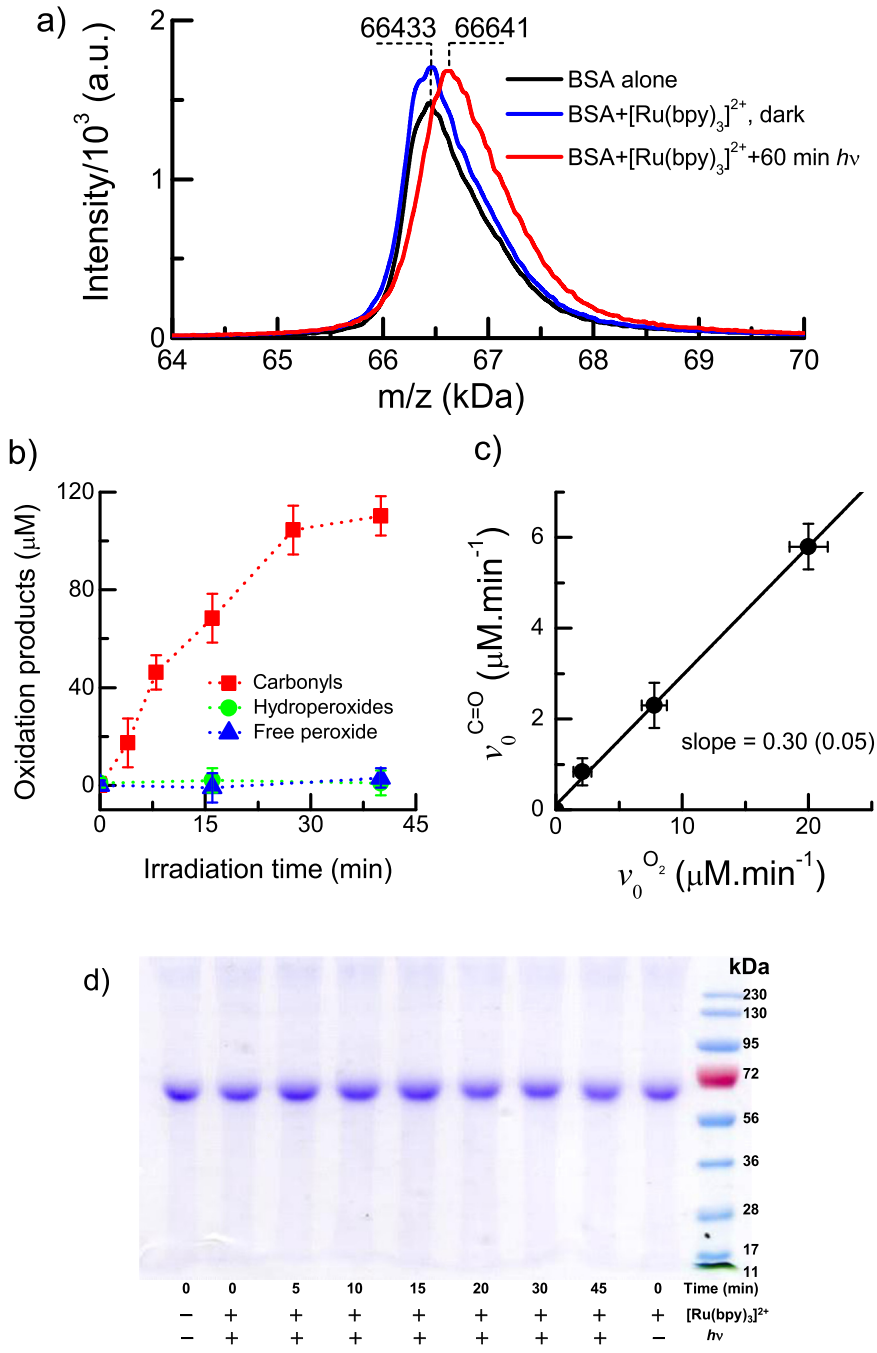

Fig. 3. (a) MALDI-TOF MS of 30 μM BSA native (black line) and in the presence of 60 μM $[Ru(bpy)_3]^{2+}$ before (blue line) and after 60 min of blue-light irradiation (red line). (b) Concentration of protein carbonyls and hydroperoxides, and free H_2O_2 produced during photo-oxidation of 100 μM BSA under steady-state irradiation with blue-LED (462 nm) of 20 μM $[Ru(bpy)_3]^{2+}$ in 50 mM Na-phosphate buffer at pH 7.4. (c) Relationship between the initial rates of protein carbonyl formation and $^3O_2$-uptake. (d) SDS-PAGE (12%) of 100 μM BSA under different irradiation conditions (MW BSA=66.4 kDa). (For interpretation of the references to color in this figure legend, the reader is referred to the web version of this article.)

in the region between 300 and 400 nm was produced without bleaching of the metal-to-ligand charge-transfer band of $[Ru(bpy)_3]^{2+}$ (Fig. 4a). This result confirms that neither direct nor photosensitized degradation of the metal complex was produced. Hence, the differential absorption spectrum after 30 min of steady-state photolysis indicates the formation of new protein chromophore(s) with maximum absorption band at ≈325 nm (inset of Fig. 4a).

Fig. 4b and c compare the photo-oxidation kinetics under identical photosensitization conditions of $[Ru(bpy)_3]^{2+}$ solutions with only ADPA and with the mixture of ADPA and BSA at the same concentrations than in the individual solution of actinometer and protein, respectively. For the irradiated solution containing both ADPA and BSA, the absorbance increment at 300–350 nm was simultaneous with the bleaching of the absorption band of ADPA due to the breakdown of the aromatic conjugation of the anthracene moiety to form the 9,10-endoperoxide derivative (Fig. S1 of Supplementary Information) [34].

However, the observed first-order constant value monitored at 380 nm for the bleaching of ADPA was reduced in a similar amount of the observed rate constant for the absorbance growth at 320 nm. This result indicates that BSA competed with ADPA to

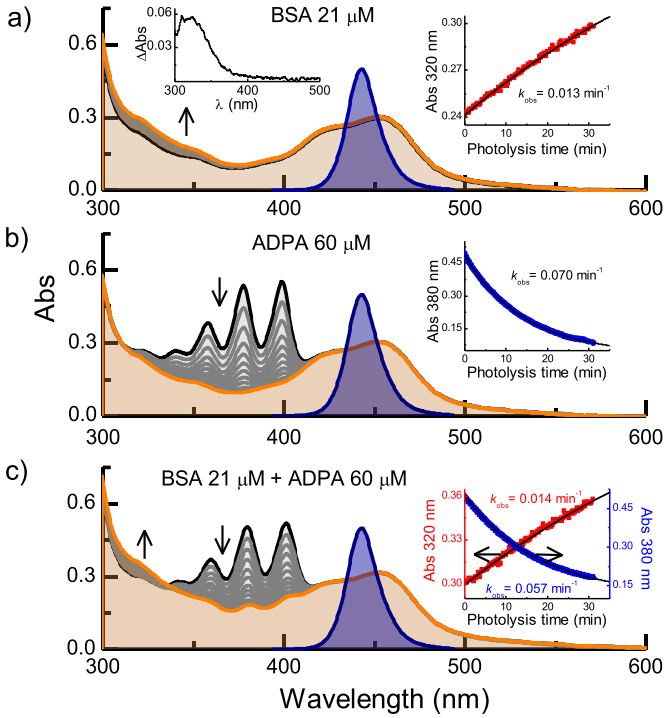

Fig. 4. Spectral changes produced during blue-LED continuous irradiation of 20 μM $[Ru(bpy)_3]^{2+}$ air-saturated solutions containing: (a) 21 μM BSA; (b) 60 μM ADPA, and (c) 21 μM BSA+60 μM ADPA. Insets: (a) differential absorption spectrum of the photolyzed solution, and (a)–(c) kinetic profiles at 320 nm and 380 nm together with first-order fit (solid black line). The blue area is the emission spectra of the 1 W blue-LED used as excitation source. (For interpretation of the references to color in this figure legend, the reader is referred to the web version of this article.)

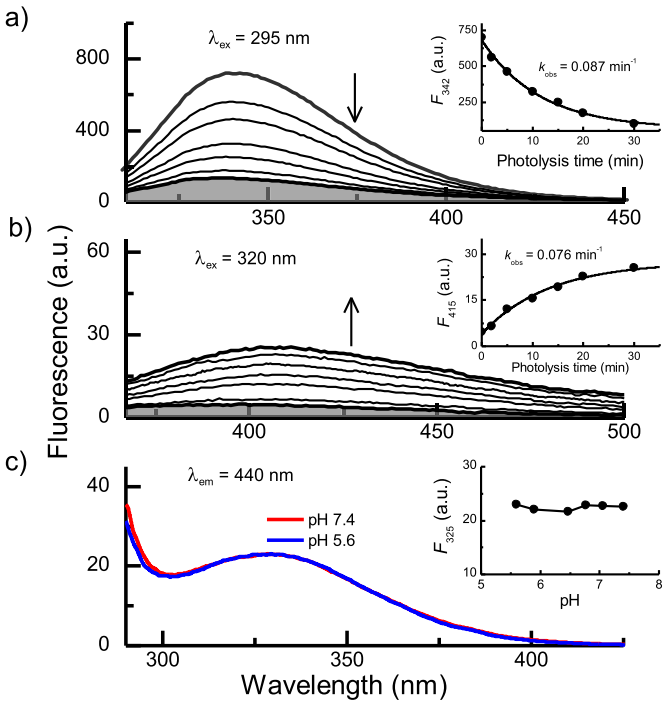

Fig. 5. Emission fluorescence spectra of 10 μM BSA air-saturated solutions as function of photolysis time of 20 μM $[Ru(bpy)_3]^{2+}$ with a blue-LED (462 nm) monitored at excitation wavelength of 295 nm (a) and 320 nm (b), with the figure insets plotting the fluorescence changes as function of photolysis time monitored at 342 nm and 410 nm, respectively. (c) pH effect on the excitation spectrum monitored with emission at 440 nm for the 30 min photo-oxidized BSA. Spectra have been corrected for the inner filter effect.

react with $^1O_2$, as expected for the reaction mechanism proposed in (Eqs. (3)–(8)), and that oxidation of BSA was only mediated by $^1O_2$ (type II mechanism).

In order to characterize the nature of the photo-oxidation product(s) associated with the new absorption band at ≈325 nm (inset Fig. 4a), the intrinsic fluorescence of BSA obtained by selective excitation at 295 nm and 320 nm was analyzed as a function of the photosensitization time. Fig. 5a shows the decreased and blue shifting (≈5 nm) of Trp-like intrinsic fluorescence of BSA during photo-oxidation. However, the excitation spectrum monitored at emission wavelength of 340 nm as function of the irradiation time only decreased without any spectral shift (Fig. S3 of Supplementary Information), suggesting that no apparent environmental modification of the vicinity near Trp residues was produced upon oxidation of BSA [45].

The progressive decrease of the Trp-like emission was accompanied by the simultaneous growth of a new emission band with maximum at ≈415 nm when the photo-oxidized solution was selectively excited at 320 nm (Fig. 5b). The similar observed rate constants k_{obs} values obtained by first-order kinetic analysis of both depletion and growth fluorescence curves suggests that these changes were kinetically linked (insets of Fig. 5a and b). Both new UV–vis and fluorescence bands arisen after BSA photo-oxidation can be potentially assigned to oxidation products of Trp, *e.g. N*′-formylkynurenine [46] and of Tyr such as dityrosine [47], since those from oxidation of Cys, Met or His are transparents in near UV and almost not fluorescents avoiding their monitoring by spectroscopic techniques. In order to probe the formation of *N*′-formylkynurenine and/or dityrosine, the pH dependence between 5.6 and 7.4 was evaluated for the excitation band of the oxidation product(s) monitored with emission at 440 nm (Fig. 5c). The excitation spectra was similar to the UV absorption band with maximum at 325 nm (inset of Fig. 4a) and independent of pH, in contrast to that observed for the excitation spectrum of dityrosine fluorophore in the same pH range [47], supporting the preliminary MS assignment that $^1O_2$-mediated oxidation of Trp residues of BSA produces *N*′-formylkynurenine, yielding two carbonyl groups by addition of two oxygen atoms per oxidized indolic ring [9,10].

At this point, the comparison of the k_{obs} values obtained by UV–vis absorbance changes for the photosensitized oxidation of BSA at 320 nm and for ADPA at 380 nm under identical photosensitization conditions (Fig. 4a and b) can be used for the calculation of the rate constant for the reaction of $^1O_2$ with both W134 and W213 residues of BSA, *i.e.* $k_{c,BSA}{}^W = 4.0(\pm 0.4) \times 10^7\ M^{-1}\ s^{-1}$. Recently, Jensen et al. [48] have shown that the Trp reactivity towards $^1O_2$ for a series of proteins bearing a single Trp residue was decreasing as the residue was deeply buried, and that for Trp located near the solvent or partially buried the reactive constant was closer to the value for the free amino acid in buffer, *e.g.* $k_c{}^W = 3 \times 10^7\ M^{-1}\ s^{-1}$ [7,8]. In the present case, slightly larger observed $k_{c,BSA}{}^W$ could suggest that $^1O_2$ can react with both W134 and W213 residues in BSA, but probably in different proportion.

To investigate the individual contribution of each Trp residues to the scavenging of $^1O_2$, BSA samples before and after 30 min of photo-oxidation were analyzed by time-resolved emission spectroscopy with pulsed excitation at 295 nm. In all cases, a global-fitting deconvolution analysis with three-exponential components in Eq. (1) was used for the fitting of the emission decay at different wavelengths, allowing the calculation of the associated fractional contributions $f_i(\lambda)$ of each decay component for determination of the decay associated spectra (DAS) with Eq. (2).

Fig. 6a shows the DAS for native (non-oxidized) BSA confirming the existence of two different Trp-like emission bands, with λ_{max} at 330 nm and 344 nm, respectively. The main fluorescence contribution (≈80% of the total spectral area) corresponded to the red-shifted band with an associated lifetime of 6.6 ns, and is

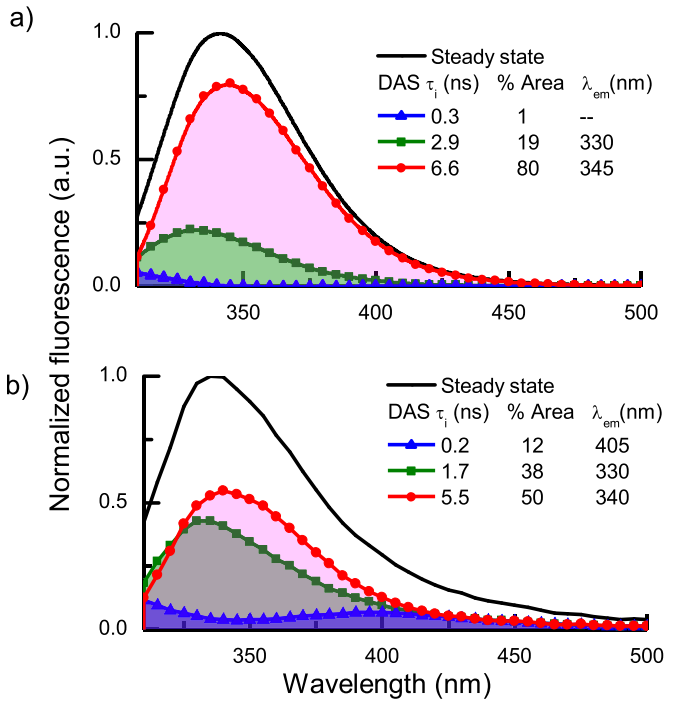

Fig. 6. Decay Associated Spectra (DAS) obtained by pulsed excitation at 295 nm of 11 μM BSA in presence of 20 μM $[Ru(bpy)_3]^{2+}$ in air-saturated solutions: (a) before, and (b) after 30 min of photo-oxidation by irradiation with blue-LED (462 nm). The associated lifetimes, emission maxima and relative band area percentage are indicated. Steady-state spectra obtained at both excitation wavelengths are indicated with black lines. The DAS were constructed by collecting fluorescence decays between 310 and 500 nm with a step of 5 nm (see Section 2).

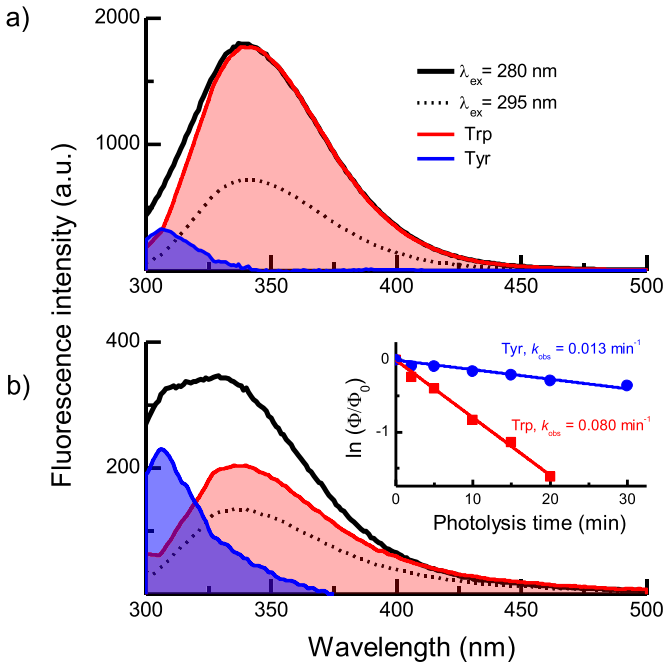

Fig. 7. Spectral deconvolution of Tyr (blue shadow) and Trp (pink shadow) emission fluorescence contribution obtained by subtracting emission spectra obtained with excitation at 280 nm (black line) and 295 nm (dotted line) with Trp normalization at 400 nm, see Ref. [50] for of 10 μM BSA air-saturated solutions in presence of 20 μM $[Ru(bpy)_3]^{2+}$ before (a) and (b) after 30 min of blue-LED photolysis. Inset: First-order plots of relative fluorescence quantum yields of Tyr (•) and Trp (▪) contribution. Spectra have been corrected for the inner filter effect. (For interpretation of the references to color in this figure legend, the reader is referred to the web version of this article.)

assigned to the W134 residue, which is a relatively solvent exposed residue located closer to the subdomain IA [12,49]. Then, the blue-shifted emission band with 19% of the total fluorescence and shorter lifetime of 2.9 ns is assigned to W213, which is more deeply buried and pointing to the cleft in the subdomain IIA or Sudlow's binding site I [13,45]. This result confirms that each Trp residue senses different nano-environment for domains I and II of BSA. The third DAS component with lifetime of 340 ps and without defined emission maximum only contributed $\leq 1\%$ to the total emission of native BSA, and it can be associated with the emission tail of residual Tyr fluorescence, since the excitation source has a half band width of ± 14 nm.

Conversely, the DAS of the oxidized BSA shows a different relative contribution of the emission bands associated with both Trp residues (Fig. 6b). As the red-shifted emission relative contribution was reduced to $\approx 50\%$ of the total fluorescence, the blue-shifted emission was increased up to $\approx 38\%$. In addition, the new emission band with maximum at 405 nm with ultra-short lifetime is associated with the formation of the side-chain *N*′-formylkynurenine derivative formed by reaction of Trp residues with $^1O_2$ [46]. By using the relative fluorescence contribution of each Trp residue in DAS in the steady-state emission spectra of BSA before and after 30 min of photo-oxidation of BSA (Fig. 5b), $\approx 90\%$ and $\approx 40\%$ of W134 and W213 were oxidized, respectively. Thus, the global photo-oxidation efficiency of Trp residues is ≈ 0.65, a similar value to that calculated for the formation of side chain *N*′-formylkynurenine using the absorbance increases at 320 nm (inset of Fig. 4a) and the reported molar absorption coefficient of $3.8 \times 10^3\ M^{-1}\ cm^{-1}$ [46].

The lower reactivity of W213 towards $^1O_2$ can be associated with the reduced diffusion and accessibility of oxygen molecules into subdomain IIA as demonstrated by the lower quenching efficiency by $^3O_2$ of the triplet excited state of the dye rose Bengal (RB), which specifically binds to this subdomain [23].

With the aim of evaluating the oxidation of Tyr residues separately from Trp ones, the steady-state fluorescence spectral deconvolution procedure proposed by Bobone et al. [50] was used. In this procedure, the spectral emission contribution of each amino acid were separated by collecting the total emission (Tyr+Trp) obtained with $\lambda_{ex}=280$ nm and subtracting the emission spectrum of Trp acquired with $\lambda_{ex}=295$ nm and matched at 400 nm, where only Trp emits, to normalize its fluorescence contribution in the total emission spectrum.

Fig. 7 illustrates the results obtained with this procedure for 10 μM BSA air-saturated solutions before and after 30 min of photosensitization with 20 μM $[Ru(bpy)_3]^{2+}$. The fluorescence emission of the native BSA obtained with excitation at 280 nm is dominated by the Trp contribution with an emission maximum at 342 nm, together with the weaker Tyr emission showing a maximum at 306 nm, due to the internal energy-transfer effect from the Tyr to Trp residues. On the contrary, after 30 min of photo-oxidation the global fluorescence emission was reduced and distorted, composed by much lower relative contribution of the Trp residues. Maximum emission band was blue-shifted at ≈ 336 nm, as already observed by both steady-state and time-resolved fluorescence with excitation at 295 nm (Figs. 5 and 6).

The inset of Fig. 7b shows the first-order plots of the relative fluorescence quantum yield of Tyr and Trp as function of the photo-oxidation time obtained from the respective deconvoluted spectra as function of the irradiation time. The same k_{obs} value for Trp degradation was obtained with this procedure as that calculated from the global emission fluorescence changes by selective excitation of Trp residues at 295 nm (inset of Fig. 5a), validating the deconvolution method used. The comparison of both k_{obs} values indicates that Tyr residues in BSA are almost 6-fold less reactive towards $^1O_2$ than Trp ones, as typically observed for the free

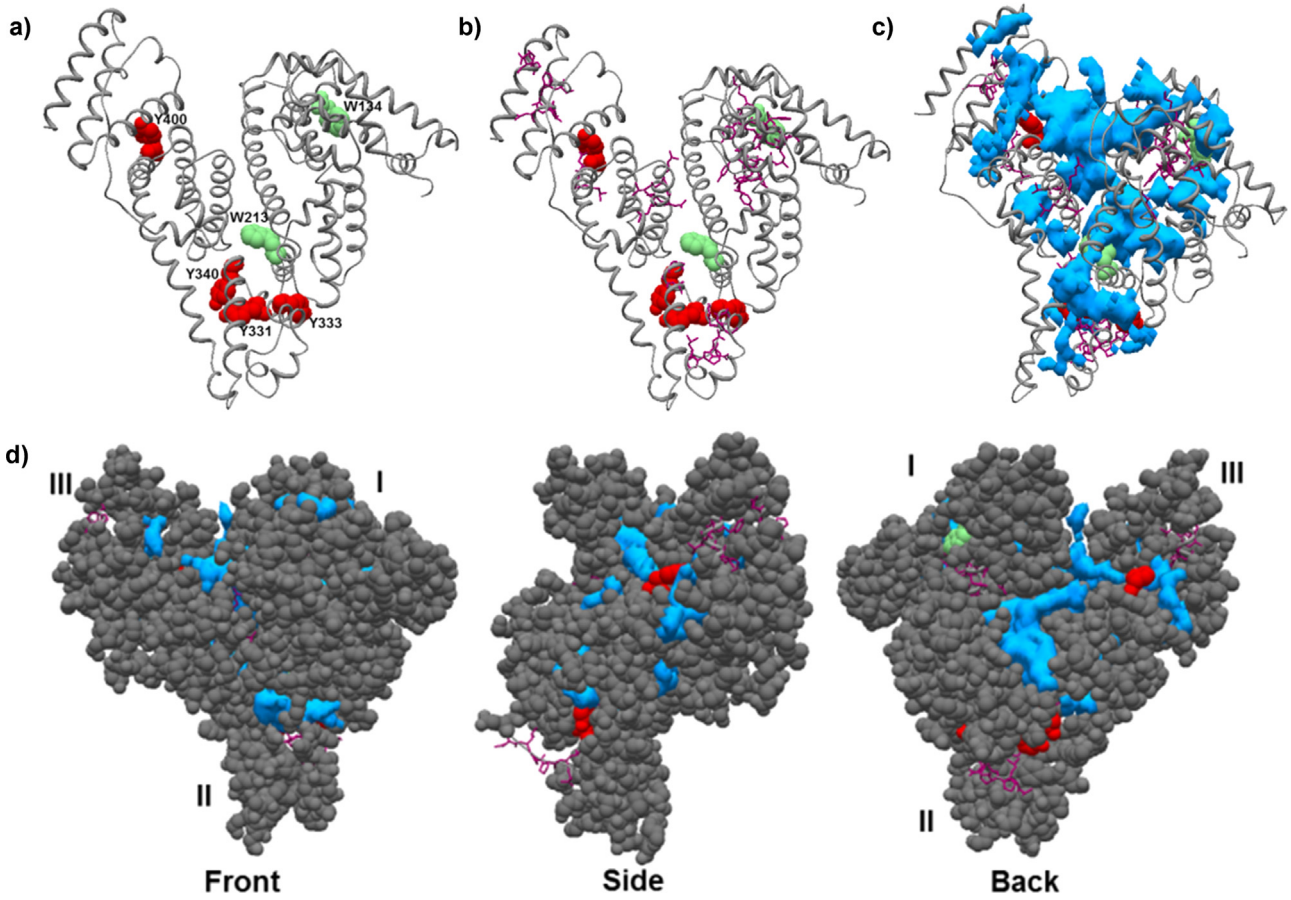

Fig. 8. 3D view of BSA obtained with the Swiss-pdb-Viewer 4.1.0 free software [51] showing: (a) $^1O_2$ oxidized residues as determined by both MALDI-TOF MS and Time-resolved fluorescence analysis (W in green balls and Y in red). (b) Hydrophobic peptide regions (as purple sticks). (c) Inner water channels through BSA (normal grooves). (d) Different views of the interconnectivity of the internal water channels with the bulk solvent. (For interpretation of the references to color in this figure legend, the reader is referred to the web version of this article.)

amino acids in aqueous media at neutral pH [7]. As MS and fluorescence experiments confirmed that two Tyr (at least) and two Trp residues per BSA were oxidized by $^1O_2$, respectively, the lower limit of the rate constant for the global chemical reaction of Tyr residues of BSA with $^1O_2$ can be estimated as $k_{c,BSA}^{Y} \geq 0.7(\pm 0.2) \times 10^7\ M^{-1}\ s^{-1}$. It can be observed that the oxidation efficiency of Tyr and Trp residues estimated as $[(k_{c,BSA}^{Y} + k_{c,BSA}^{W})/k_c^{BSA}]$ only represented about 20% of the global oxidation process, suggesting also that other reactive residues such as Met and His residues might contribute to the $^1O_2$-trapping by BSA [3,10].

3.4. BSA nano-heterogeneity effect on the compartmentalization and reactivity of $^1O_2$

Fig. 8a shows the 3D modeling of BSA (pdb 3V03) obtained with the Swiss-Pdb-Viewer 4.1.0 free software [51], indicating the distribution of the confirmed oxidized residues discussed above, e.g. W134, W213, Y331 (or Y333) and Y400. The inclusion of Y340 was only done for descriptive purposes, since its assessment MS (and of H337) were within the instrumental error. It can be observed that $^1O_2$ generated in the bulk solvent by photosensitization of $[Ru(bpy)_3]^{2+}$ is able to diffuse towards BSA and interacts with both solvent exposed and buried residues disseminated through the whole albumin. The $^1O_2$-targeting of more deeply buried residues as W213 can be assisted by the existence of highly hydrophobic peptide portions closer to those residues, given the 10-fold larger solubility of $^3O_2$ (and also $^1O_2$) in non-polar media than in water [52]. Fig. 8b shows as purple sticks the peptide regions with relative hydrophobicity > 0.6 as defined by Black and Mould [53], and calculated with the free software Protscale [54] (Fig. S4 of Supplementary Material). Fig. 8c shows the Swiss-Pdb-Viewer modeling of the inner water channels (blue shadow) conformed by solvent volumes large enough (> 100 Å^3) to accommodate oxygen molecules (molecular volume 51 Å^3/molecule [56]). Fig. 8d illustrates the interconnectivity of those inner water channels with the protein surface from different sides. This modeling approach fits well with the observed results, since it indicates the possibility of internal diffusion of $^1O_2$ generated in the bulk solvent through the whole BSA. The average radial distance that $^1O_2$ can travel during its lifetime τ_Δ° can be estimated as $d=(6Dt)^{1/2}$, where $D=2\times10^{-5}$ cm^2/s is the diffusion coefficient of $^1O_2$ in water at room temperature and $t \approx 5 \times \tau_\Delta^\circ$ is the average travel time of the species [55]. Thus, a distance $d \approx 500$ nm was calculated considering $\tau_\Delta^\circ = 3.1$ μs as the $^1O_2$ lifetime value in water in the absence of quenchers [4]. This traveled distance represents a spherical diffusional volume of several orders of magnitude larger than the molecular volume of BSA [13], allowing the diffusion of $^1O_2$ through several BSA molecules during its lifetime. It is interesting to note that the bulkier hydrophobic peptide regions in domains I and II are delimited or closer to some Met and His, probably facilitating their interaction with $^1O_2$.

As suggested by Molecular Dynamics simulations for molecular oxygen in ns-time window [56,57], hydrophobic residues located on cavities on the protein surface are used to capture oxygen molecules from the bulk solvent. After a short period residing there, they seem to move to inner cavities through one or more channels. Taking this into account, singlet oxygen behavior can

also be explained in a similar fashion. Plotting residues according to their hydrophobicity and those oxidized, a clear pattern emerges. Whether this association is related to a "walking path" of singlet oxygen from grooves through the protein surface towards hydrophobic residues and then quenched by reactive residues, such as Trp or Tyr, or if this pattern is merely coincidental is a topic that needs to be addressed. We are currently working on the optimization of mass spectrometric analyses to evidence all possible oxidation sites since the abundance of certain candidate ions did not allow us to confirm their identity using MS/MS. This data together with molecular dynamics simulations might explain the route of singlet oxygen from bulk solvent to specific hydrophobic areas on the protein surface and the distribution pattern of oxidations observed.

4. Conclusions

Photosensitized oxidations contribute to biological damage induced, through processes involving the generation of radical species (type I mechanism), for example, by electron transfer or hydrogen abstraction, and/or the production of $^1O_2$ (type II mechanism). Here, the photosensitized oxidation of BSA using $[Ru(bpy)_3]^{2+}$ as sensitizer in air-saturated Na-phosphate buffer solution was evaluated by kinetic and spectroscopic methods. As both ground and excited states of the sensitizer did not interact with the protein, the oxidation of BSA was exclusively mediated by $^1O_2$ produced in the solution. In turns, BSA quenched efficiently $^1O_2$ with a total (physical+chemical) quenching rate constant $k_t^{BSA}=7.3(\pm 0.4)\times 10^8\ M^{-1}\ s^{-1}$, with $\approx$40% of chemical pathway contribution, *i.e.* $k_c^{BSA}=2.7(\pm 0.9)\times 10^8\ M^{-1}\ s^{-1}$. Both k_t^{BSA} and k_c^{BSA} values are typically found for albumins and indicate that several residues interact in parallel with $^1O_2$. Among those residues, oxidation of W134 and W213 resulted in the formation of the fluorescent side-chain *N′*-formylkynurenine, with an global reaction rate constant $k_{c,BSA}{}^{W}=4.0(\pm 0.4)\times 10^7\ M^{-1}\ s^{-1}$. Time-resolved emission spectra analysis confirmed that the solvent exposed W134 was more efficiently oxidized by $^1O_2$ than the buried W213, due to the environmental nano-heterogeneity difference between BSA subdomains. MS analysis indicated that at least two Tyr residues were oxidized by $^1O_2$ to form DOPA by adding one oxygen atom per residue. Steady-state deconvolution of the emission spectrum of BSA indicated than Tyr residues were less reactive towards $^1O_2$ than Trp with $k_{c,BSA}{}^{Y}\geq 0.7(\pm 0.2)\times 10^7\ M^{-1}\ s^{-1}$. The analysis of kinetic data together with the relatively low efficiency of formation of protein carbonyls ($\approx$30%) suggested that residues other than Trp and Tyr; e.g. Met and His; must be also oxidized by $^1O_2$.

The observed oxidative pattern of BSA can be better understood by compartmentalization effects of $^1O_2$ as a result of the nano-heterogeneity of the albumin. The modeling of 3D-structure of BSA indicates the presence of interconnected hydrophilic grooves and hydrophobic peptide patches at the interior of the protein where $^1O_2$ can be able to diffuse from the bulk solvent during its lifetime, reaching buried amino acids such as W213.

This study confirms that highly diffusive reactive species, such as $^1O_2$, are able to be dispersed into the interior of bulky proteins by the presence of interconnected hydrophilic and hydrophobic regions. This nano-compartmentalization can produce intricate oxidation patterns involving the degradation of both solvent exposed and buried residues.

Acknowledgments

This research was supported by the bi-national cooperation program ARC/11/15 of MINCyT (Argentina) and 7AMB12AR028 of MEYS (Czech Republic). We also thank to Dr. Ondrej Šedo and Assoc. Prof. Zbyněk Zdráhal from Central European Institute of Technology (CEITEC) in Brno, Czech Republic, for MALDI-TOF mass spectrometry experiments carried out with the support of Proteomics Core Facility of CEITEC, ID no. CZ.1.05/1.1.00/02.0068, financed from European Regional Development Fund and grant of the Grant Agency of the Czech Republic P206/12/G151. C.D.B. also thanks the Argentinean funding institutions CONICET (PIP 0374/12), FONCyT (PICT-2012-2666) and UNSE (PICTO-2012-0013).

Appendix A. Supplementary material

Supplementary data associated with this article can be found in the online version at http://dx.doi.org/10.1016/j.freeradbiomed.2015.11.014.

References

[1] S.I. Liochev, Reactive oxygen species and the free radical theory of aging, Free Rad. Biol. Med. 60 (2013) 1–4.
[2] B.S. Berlett, E.R. Stadtman, Protein oxidation in aging, disease, and oxidative stress, J. Biol. Chem. 272 (1997) 20313–20316.
[3] M.J. Davies, The oxidative environment and protein damage, Biochim. Biophys. Acta-Proteins Proteom 1703 (2005) 93–109.
[4] C. Schweitzer, R. Schmidt, Physical mechanisms of generation and deactivation of singlet oxygen, Chem. Rev. 103 (2003) 1685–1757.
[5] P. Di Mascio, E.J.H. Bechara, M.H.G. Medeiros, K. Briviba, H. Sies, Singlet molecular oxygen production in the reaction of peroxynitrite with hydrogen peroxide, FEBS Lett. 355 (1994) 287–289.
[6] M. Tarr, D.P. Valenzeno, Singlet oxygen: the relevance of extracellular production mechanisms to oxidative stress in vivo, Photochem. Photobiol. Sci. 2 (2003) 355–361.
[7] E.A. Lissi, M.V. Encinas, E. Lemp, M.A. Rubio, Singlet oxygen $O_2(^1\Delta_g)$ bimolecular processes. solvent and compartmentalization effects, Chem. Rev. 93 (1993) 699–723.
[8] F. Wilkinson, J.G. Brummer, Rate constants for the decay and reactions of the lowest electronically excited singlet state of molecular oxygen in solution, J. Phys. Chem. Ref. Data 10 (1981) 809–999.
[9] M.J. Davies, Singlet oxygen-mediated damage to proteins and its consequences, Biochem. Biophys. Res. Commun. 305 (2003) 761–770.
[10] D.I. Pattison, A.S. Rahmanto, M.J. Davies, Photo-oxidation of proteins, Photochem. Photobiol. Sci. 11 (2012) 38–53.
[11] G. Fanali, A. di Masi, V. Trezza, M. Marino, M. Fasano, P. Ascenzi, Human serum albumin: from bench to bedside, Mol. Asp. Med. 33 (2012) 209–290.
[12] T. Peters, All About Albumin Proteins, Academic Press, New York, 1996.
[13] K.A. Majorek, P.J. Porebski, A. Dayal, M.D. Zimmerman, K. Jablonska, A. J. Stewart, M. Chruszcz, W. Minor, Structural and immunologic characterization of bovine, horse, and rabbit serum albumins, Mol. Immunol. 52 (2012) 174–182.
[14] L. Musante, M. Bruschi, G. Candiano, A. Petretto, N. Dimasi, P.D. Boccio, A. Urbani, G. Rialdi, G.M. Ghiggeri, Characterization of oxidation end product of plasma albumin 'in vivo', Biochem. Biophys. Res. Commun. 349 (2006) 668–673.
[15] M. Roche, P. Rondeau, N.R. Singh, E. Tarnus, E. Bourdon, The antioxidant properties of serum albumin, FEBS Lett. 582 (2008) 1783–1787.
[16] G. Aldini, G. Vistoli, L. Regazzoni, L. Gamberoni, R.M. Facino, S. Yamaguchi, K. Uchida, M. Carini, Albumin is the main nucleophilic target of human plasma: a protective role against pro-atherogenic electrophilic reactive carbonyl species? Chem. Res. Toxicol. 21 (2008) 824–835.
[17] B. Alvarez, S. Carballal, L. Turell, R. Radi, Formation and reactions of sulfenic acid in human serum albumin, Methods Enzymol. 473 (2010) 117–136.
[18] G. Colombo, M. Clerici, D. Giustarini, R. Rossi, A. Milzani, I. Dalle-Donne, Redox albuminomics: oxidized albumin in human diseases, Antioxid. Redox Signal. 17 (2012) 1515–1527.
[19] J.A. Silvester, G.S. Timmins, M.J. Davies, Protein hydroperoxides and carbonyl groups generated by porphyrin-induced photo-oxidation of bovine serum albumin, Arch. Biochem. Biophys. 350 (1998) 249–258.
[20] E. Alarcon, A.M. Edwards, A.M. Garcia, M. Munoz, A. Aspee, C.D. Borsarelli, E. A. Lissi, Photophysics and photochemistry of zinc phthalocyanine/bovine serum albumin adducts, Photochem. Photobiol. Sci. 8 (2009) 255–263.
[21] E. Alarcon, A.M. Edwards, A. Aspee, F.E. Moran, C.D. Borsarelli, E.A. Lissi, D. Gonzalez-Nilo, H. Poblete, J.C. Scaiano, Photophysics and photochemistry of dyes bound to human serum albumin are determined by the dye localization, Photochem. Photobiol. Sci. 9 (2010) 93–102.
[22] J.A. Silvester, G.S. Timmins, M.J. Davies, Photodynamically generated bovine serum albumin radicals: evidence for damage transfer and oxidation at

cysteine and tryptophan residues, Free Radic. Biol. Med. 24 (1998) 754–766.
[23] M.B. Espeche Turbay, V. Rey, N.M. Argañaraz, F.E. Morán Vieyra, A. Aspée, E. A. Lissi, C.D. Borsarelli, Effect of dye localization and self-interactions on the photosensitized generation of singlet oxygen by rose bengal bound to bovine serum albumin, J. Photochem. Photobiol. B: Biol. 141 (2014) 275–282.
[24] A.K. Covington, M. Paabo, R.A. Robinson, R.G. Bates, Use of the glass electrode in deuterium oxide and the relation between the standardized pD (paD) scale and the operational pH in heavy water, Anal. Chem. 40 (1968) 700–706.
[25] R.L. Levine, J.A. Williams, E.R. Stadtman, E. Shacter, Carbonyl assays for determination of oxidatively modified proteins, Methods Enzymol. 233 (1994) 346–357.
[26] R. Bou, R. Codony, A. Tres, E.A. Decker, F. Guardiola, Determination of hydroperoxides in foods and biological samples by the ferrous oxidation–xylenol orange method: a review of the factors that influence the method's performance, Anal. Biochem. 377 (2008) 1–15.
[27] C.C. Allain, L.S. Poon, C.S.G. Chan, W. Richmond, P.C. Fu, Enzymatic determination of total serum cholesterol, Clin. Chem. 20 (1974) 470–475.
[28] M.I. Gutierrez, C.G. Martinez, D. Garcia-Fresnadillo, A.M. Castro, G. Orellana, A. M. Braun, E. Oliveros, Singlet oxygen ($^1\Delta_g$) production by ruthenium(II) complexes in microheterogeneous systems, J. Phys. Chem. A 107 (2003) 3397–3403.
[29] A.A. Abdel-Shafi, P.D. Beer, R.J. Mortimer, F. Wilkinson, Photosensitized generation of singlet oxygen from (substituted bipyridine)ruthenium(II) complexes, Helv. Chim. Acta 84 (2001) 2784–2795.
[30] Q.G. Mulazzani, H. Sun, M.Z. Hoffman, W.E. Ford, M.A.J. Rodgers, Quenching of the excited states of ruthenium(II)-diimine complexes by oxygen, J. Phys. Chem. 98 (1994) 1145–1150.
[31] R.B. Thompson, I. Gryczynski, J. Malicka, Fluorescence polarization standards for high-throughput screening and imaging, Biotechniques 32 (2002) 34–42.
[32] C.D. Borsarelli, H. Corti, D. Goldfarb, S.E. Braslavsky, Structural volume changes in photoinduced electron transfer reactions. Laser-induced optoacoustic studies of speciation during the quenching reaction of excited $Ru(bpy)_3^{2+}$ by Fe (III) in aqueous solutions, J. Phys. Chem. A 101 (1997) 7718–7724.
[33] C.D. Borsarelli, unpublished results.
[34] M.J. Moreno, E. Monson, R.G. Reddy, A. Rehemtulla, B.D. Ross, M. Philbert, R. J. Schneider, R. Kopelman, Production of singlet oxygen by $Ru(dpp(SO_3)_2)_3$ incorporated in polyacrylamide PEBBLES, Sensors Actuat. B: Chem. 90 (2003) 82–89.
[35] F.E. Scully Jr, J. Hoigné, Rate constants for reactions of singlet oxygen with phenols and other compounds in water, Chemosphere 16 (1987) 681–694.
[36] R.L. Jensen, J. Arnbjerg, H. Birkedal, P.R. Ogilby, Singlet oxygen's response to protein dynamics, J. Am. Chem. Soc. 133 (2011) 7166–7173.
[37] R.H. Bisby, C.G. Morgan, I. Hamblett, A.A. Gorman, Quenching of singlet oxygen by trolox C, Ascorbate, and amino acids: effects of pH and temperature, J. Phys. Chem. A 103 (1999) 7454–7459.
[38] I.B.C. Matheson, J. Lee, Chemical reaction rates of amino acids with singlet oxygen, Photochem. Photobiol. 29 (1979) 879–881.
[39] A. Michaeli, J. Feitelson, Reactivity of singlet oxygen toward amino acids and peptides, Photochem. Photobiol. 59 (1994) 284–289.
[40] M.J. Davies, Reactive species formed on proteins exposed to singlet oxygen, Photochem. Photobiol. Sci. 3 (2004) 17–25.
[41] D.N. Perkins, D.J.C. Pappin, D.M. Creasy, J.S. Cottrell, Probability-based protein identification by searching sequence databases using mass spectrometry data, Electrophoresis. 20 (1999) 3551–3567.
[42] E. Alarcon, A.M. Edwards, A. Aspee, C.D. Borsarelli, E.A. Lissi, Photophysics and photochemistry of rose bengal bound to human serum albumin, Photochem. Photobiol. Sci. 8 (2009) 933–943.
[43] A. Wright, W.A. Bubb, C.L. Hawkins, M.J. Davies, Singlet oxygen-mediated protein oxidation: evidence for the formation of reactive side chain peroxides on tyrosine residues, Photochem. Photobiol. 76 (2002) 35–46.
[44] V. Vargová, R.E. Giménez, H. Černocká, D.C. Trujillo, F. Tulli, V.I.P. Zanini, E. Paleček, C.D. Borsarelli, V. Ostatná, Label-free electrochemical detection of singlet oxygen protein damage, Electrochim. Acta **187** (2016) 662–669.
[45] N. Tayeh, T. Rungassamy, J.R. Albani, Fluorescence spectral resolution of tryptophan residues in bovine and human serum albumins, J. Pharmaceut. Biomed. Anal. 50 (2009) 107–116.
[46] Y. Fukunaga, Y. Katsuragi, T. Izumi, F. Sakiyama, Fluorescence characteristics of kynurenine and *N*′-formylkynurenine. Their use as reporters of the environment of tryptophan 62 in hen egg-white lysozyme, J. Biochem. 92 (1982) 129–141.
[47] D.A. Malencik, S.R. Anderson, Dityrosine as a product of oxidative stress and fluorescent probe, Amino Acids 25 (2003) 233–247.
[48] R.L. Jensen, J. Arnbjerg, P.R. Ogilby, Reaction of singlet oxygen with tryptophan in proteins: A pronounced effect of the local environment on the reaction rate, J. Am. Chem. Soc. 134 (2012) 9820–9826.
[49] G.J. van der Vusse, Albumin as fatty acid transporter, Drug Metab. Pharmacok. 24 (2009) 300–307.
[50] S. Bobone, M. van de Weert, L. Stella, A reassessment of synchronous fluorescence in the separation of Trp and Tyr contributions in protein emission and in the determination of conformational changes, J. Mol. Struct. 1077 (2014) 68–76.
[51] N. Guex, M.C. Peitsch, Swiss-model and the Swiss-PdbViewer: an environment for comparative protein modeling, Electrophoresis 18 (1997) 2714–2723.
[52] R. Battino, T.R. Rettich, T. Tominaga, The solubility of oxygen and ozone in liquids, J. Phys. Chem. Ref. Data 12 (1983) 163–178.
[53] S.D. Black, D.R. Mould, Development of hydrophobicity parameters to analyze proteins which bear post- or cotranslational modifications, Anal. Biochem. 193 (1991) 72–82.
[54] E. Gasteiger, C. Hoogland, A. Gattiker, S. Duvaud, M.R. Wilkins, R.D. Appel, A. Bairoch, Protein identification and analysis tools on the ExPASy server, in: J. M. Walker (Ed.), The Proteomics Protocols Handbook, Humana Press, 2005, pp. 571–607.
[55] P.R. Ogilby, Singlet oxygen: there is indeed something new under the sun, Chem. Soc. Rev. 39 (2010) 3181–3209.
[56] R. Baron, C. Riley, P. Chenprakhon, K. Thotsaporn, R.T. Winter, A. Alfieri, F. Forneris, W.J. van Berkel, P. Chaiyen, M.W. Fraaije, A. Mattevi, J. A. McCammon, Multiple pathways guide oxygen diffusion into flavoenzyme active sites, Proc. Natl. Acad. Sci. USA 106 (2009) 10603–10608.
[57] C.K. Regmi, Y.R. Bhandari, B.S. Gerstman, P.P. Chapagain, Exploring the diffusion of molecular oxygen in the red fluorescent protein mCherry using explicit oxygen molecular dynamics simulations, J. Phys. Chem. B. 117 (2013) 2247–2253.